8-2015

Similarity Analysis of a Swirling Counter-Flow

Jitesh Rane

SIMILARITY ANALYSIS OF A SWIRLING COUNTER-FLOW

A Thesis

Submitted to the Faculty

of

Embry-Riddle Aeronautical University

by

Jitesh Rane

In Partial Fulfillment of the

Requirements for the Degree

of

Master of Science in Aerospace Engineering

August 2015

Embry-Riddle Aeronautical University

Daytona Beach, Florida

SIMILARITY ANALYSIS OF A SWIRLING COUNTER-FLOW

by

Jitesh Rane

A Thesis prepared under the direction of the candidate's committee chairman, Dr. Yechiel Crispin, Department of Aerospace Engineering, and has been approved by the members of the thesis committee. It was submitted to the School of Graduate Studies and Research and was accepted in partial fulfillment of the requirements for the degree of Master of Science in Aerospace Engineering.

THESIS COMMITTEE

Chairman, Dr. Yechiel Crispin

Member, Dr. Reda Mankbadi

Member, Dr. Dongeun Seo

Department Chair, Dr. Anastasios Lyrintzis
or Graduate Program Coordinator, Dr. Eric Perrell

25 Aug 15
Date

Dean of College of Engineering, Dr. Maj Mirmirani

08/29/15
Date

Associate VP for Academics, Dr. Christopher Grant

9/2/15
Date

ACKNOWLEDGMENTS

First of all, I would like to thank my thesis advisor Dr. Yechiel Crispin for his continued guidance and support from the moment I started this course. He has been very helpful and understanding and this would not have been possible without his help.

I would also like to thank all the faculty members in the Aerospace Engineering department of Embry-Riddle Aeronautical University for having their doors and ears open for me whenever I needed their help.

Also a thanks to all my friends, here at ERAU and also back home, especially the TRFC folks, mostly for their comic support and entertainment skills.

And my parents, without whom I would never have reached this stage in my life. Their continued moral and financial support has kept me motivated throughout my life and I am forever indebted to them. And to my extended family, for being so awesome.

TABLE OF CONTENTS

LIST OF FIGURES

SYMBOLS

r	radius
t	time
v	velocity
v_r	radial component of velocity
v_ϕ	tangential component of velocity
v_z	axial component of velocity
z	axial direction
ϕ	tangential direction
P	pressure
μ	viscosity
ρ	density
R_{in}	inner radius of cylinder
$v_{\phi sc}$	characteristic swirl velocity
Re	reynolds number
ν	kinematic viscosity
ψ	stream function
λ	swirl decay rate in z-direction
H	height/length of the cylinder
R	radius of the cylinder
ω	angular velocity

ABBREVIATIONS

VBB	vortex breakdown bubble
VIHRE	vortex injection hybrid rocket engine
CFD	computational fluid dynamics
2D	two dimensional
3D	three dimensional

ABSTRACT

Rane, Jitesh MSAE, Embry-Riddle Aeronautical University, August 2015. Similarity Analysis of a Swirling Counter-flow.

Swirling counter-flows are used in numerous engineering applications, like combustion, heat exchangers, cyclonic separation and mixing, etc. These swirling counter-flows produce complex flow fields. It is important to study these types of flows in order to be able to use them properly in many applications.

The present work provides insight into the flowfield inside a swirling counter-flow when the fluid is injected tangentially in a cylindrical container. A semi-analytical solution is developed by starting with the full Navier-Stokes equations and using a similarity analysis. A decaying swirl along the axis of the cylinder is assumed, which reduces the Navier-Stokes equations to first order ordinary differential equations with boundary conditions. The two point boundary value and eigenvalue problem is then solved using a collocation method. Profiles are obtained for various velocity components that validate the swirling counter-flow behavior. The opposite pressure gradients near the inlet and dead-end, and also near the side wall and the axis, show that there are two streams of fluids that flow in opposite directions. CFD simulations of 2D axisymmetric setup and a full 3D configuration of the same problem are carried out using a commercial finite volume method code (Fluent). The analytical results are then compared against the CFD results. It is observed that the velocity profiles for all the cases behave similarly, although there are some variations in their values.

1. Introduction

Swirling flows have many interesting features and occur frequently both in nature and in technology. The main interest for these kind of flows developed due to the need to study the flows of tornados which cause severe damage and are one of the most dangerous natural calamities. Swirling flow is an important natural as well as technological phenomena. They have found applications in combustion, heat exchange, cyclone separation, mixing, etc. The complex nature of the flow however hinders the complete understanding and hence, an efficient application to recent technologies. For these reasons, swirling flows have been extensively studied over several decades. Many publications and books can be found in the literature that give a thorough review of swirling flows (Gupta, Lilley, & Syred, 1984); (Steenbergen, 1995); (Rocklage-Marliani, Schmidts, & Ram, 2003) ; (Pashtrapanska, Jovanovic, Lienhart, & Durst, 2006). Most of these studies concentrate on the effects of swirl flow created when the fluid is subjected to sudden or gradual expansion in pipes or injected as a free jet. It is observed that the swirl component decays as you go downstream because of adverse pressure gradients and vortex breakdowns are observed.

1.1 Background on Swirling Flows

Swirl flows can be said to be a combination of axial motion and tangential motion. As a result, the fluid moves forward in a helical path. Various swirl-generating methods can be used to generate swirl flows that impart spiral motion to a laminar flow. (Gupta et al., 1984) classified them into 3 principal categories.

1. Tangential inlets, such as tangential plus axial entry or just tangential slots.

2. Guided vanes such as swirl vane packs, swirlers, honeycomb structures.

3. Direct rotation such as rotating pipes.

As the fluid passes through the swirl generators, the previously non-swirling flow acquires helical streamlines. The fluid moves in helical paths and may be considered as a combination of primary and secondary flows. The primary flow is parallel to the longitudinal axis whereas the secondary flow is a circulatory fluid motion about the axes parallel to the primary flow. (Fokeer, 2006)

There is no standard quantity that denotes the strength of a swirling flow. However, the swirl number S is commonly used. The definition of swirl number varies from author to author. (Gupta et al., 1984) defines the Swirl number as a nondimensional number representing the angular momentum flux of the fluid divided by the axial momentum flux and the hydraulic radius of the pipe in which swirl flow occurs.

$$S = \frac{G_\theta}{G_x R} \tag{1.1}$$

where,

$$G_\theta = \int (\rho u_x u_\theta + \rho\overline{u''_x u''_\theta}) r^2 dr \tag{1.2}$$

and

$$G_x = \int_0^R (\rho u_x^2 + \rho\overline{u'^2} + (p - p_\infty)) r dr \tag{1.3}$$

It is difficult to calculate the exct swirl number with these equations since it is very hard to get the pressure and velocity values experimentally. Simplification to these equations can be found easily in the literature. Another much more widely used definition is given by (Rocklage-Marliani et al., 2003) as

$$S = \frac{\int_0^R u_x u_\theta r^2 dr}{R \int_0^R u_x^2 r dr} \tag{1.4}$$

This equation was further simplfied by (Rocklage-Marliani et al., 2003)., as

$$S = \frac{2 \int_0^R u_x u_\theta r^2 dr}{R^3 u_{ref}^2} \tag{1.5}$$

where the axial momentum flux is replaced by a reference velocity uref.

(Parchen & Steenbergen, 1998) showed that swirl intensity, defined by Eq. 1.5, decays exponentially as:

$$S = S_0 e^{-\frac{\beta x}{D}} \tag{1.6}$$

where β is the decay rate and S_0 is the initial swirl intensity.

1.2 Counterflows

Counterflows, which are flows of a fluid in opposite directions have a wide number of technological applications. There are two types of counterflows: flows in the opposite direction separated by an impermeable surface and flows with no separating surface. Heat exchangers use an impermeable surface between the fluids flowing in the opposite direction, to facilitate the transfer of heat but keeping the hot and cold fluids separated at all times. Hydrocyclones, vortex tubes and vortex combustors are examples of counterflows that have no separating surfaces between the flows. A natural example of a counterflow is the Gulf Stream in the Atlantic Ocean, where opposite currents occur in the ocean depths. These flows are highly turbulent but still survive intense mixing. Swirling counterflows are used in vortex combustors to efficiently mix fuel, oxidizer, and flue gases. Efficiency increases as a result of the swirling flows and also reduces harmful emissions. Vortex tubes and commercial hydrocyclones also work on the principles of swirling counterflows.

1.3 Mechanism of Swirling Counterflows

The mechanism of swirling counterflows is based upon a pressure minimum occuring at the focal point near the axis (Shtern, 2012). Here, the cyclostrophic balance equation, $\partial p/\partial r = \rho v_s^2/r$ comes into play, which is the relation between the centrifugal force and the radial gradient of pressure. The equation shows that pressure increases as we move away from the axis, since $\rho v_s^2/r$ is always > 0.

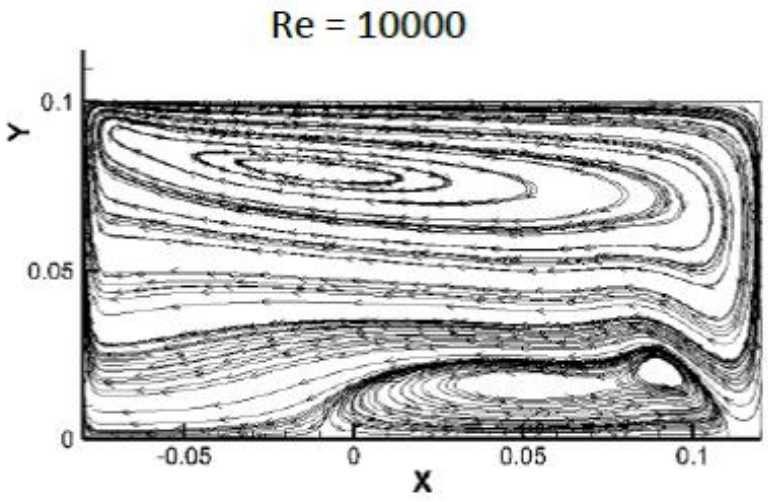

Figure 1.1. Vortex Breakdown Bubble in a fluid filled cylinder with endwall rotation, for Re=10000.

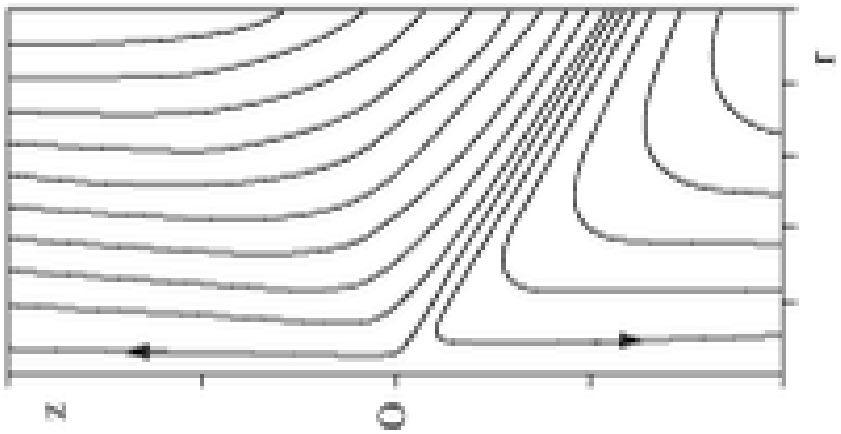

Figure 1.2. Close up of streamlines of a vortex breakdown bubble

Now for the axial pressure gradient, consider the flow shown in figure 1.2 (Shtern, 2012), where the z direction represents the axis of rotation and the horizontal axis represents the radial direction. For a high speed flow, the angular momentum rv_s is almost completely conserved along a streamline. Thus, as the streamline approaches

near the axis, the swirl velocity increases and the pressure drops at the axis according to the cyclostrophic balance equation.

Near the focal point, the streamlines first converge near the axis, then diverge away from the axis. A local pressure minimum is developed at the axial location where the flow convergence changes into flow divergence. As the swirl velocity increases, the pressure minimum becomes deeper and deeper, and thus starts to suck fluid from downstream. As a result, this causes flow reversal and swirl-induced circulation, which is referred to as vortex-breakdown bubble, VBB. This swirl-induced counterflow is on a local scale, and is small compared to the surrounding flow.

On a larger scale, however, swirl causes global meridional circulation, occupying the entire flow region. Flows where both global and local circulations occur are common. An example of this shown in figure 1.1, from a CFD simulation conducted by the author(and is also analyzed in detail later in this thesis). Figure 1.1 shows an axisymmetric setup of a sealed cylinder filled with fluid, with one rotating endwall. The fluid moves along the sidewall towards the deadend, makes a U-turn and moves back towards the rotating end along the axis, which is the global circulation of the system. For a certain swirl intensity, VBB is observed near the axis, as shown in the figure. This is the local circulation.

1.4 Applications of Swirling Counterflows

As stated previously, swirling counterflows have found applications in hydrocyclones, vortex tubes, vortex combustors, etc. The flows moving in opposite directions

are used to seperate solid particles suspended in liquids or two liquids of different densities.

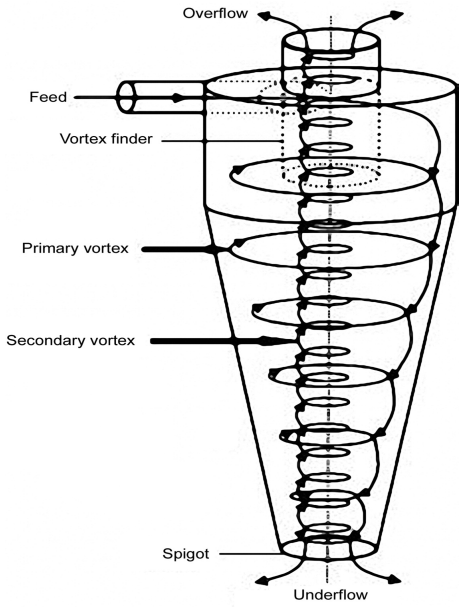

Figure 1.3. Schematic of a hydrocyclone (Ozgen & Yildiz, 2010).

Figure 1.3 (Ozgen & Yildiz, 2010) shows a schematic of a hydrocylone. The mixture to be separated, lets say oil-water mixture (Shtern, 2012) is injected tangentially and develops a swirling flow. The mixture travels along the length, where the oil droplets are pushed into the inner vortex due to centrifugal buoyancy, which again travels back up and exits through the overflow. The clean water exits through the underflow. A similar application is found in vortex tubes where pressurized air is injected tangentially to be separated into hot and cold outflows.

The most recent application of swirling counterflows has been in the field of rocket motors. Hybrid rockets, which use solid fuel and liquid oxidizer for propulsion, are considered as an attractive and viable alternative to liquid and solid rockets due to a

large number of safety, cost and ease of manufacture advantages. However, they face a few disadvantages (Chiaverini & Kuo, 2007) such as low regression rate of solid fuel, low volumetric loading, and low combustion efficiency. Swirl injection of oxidizer is considered as a solution to these problems.

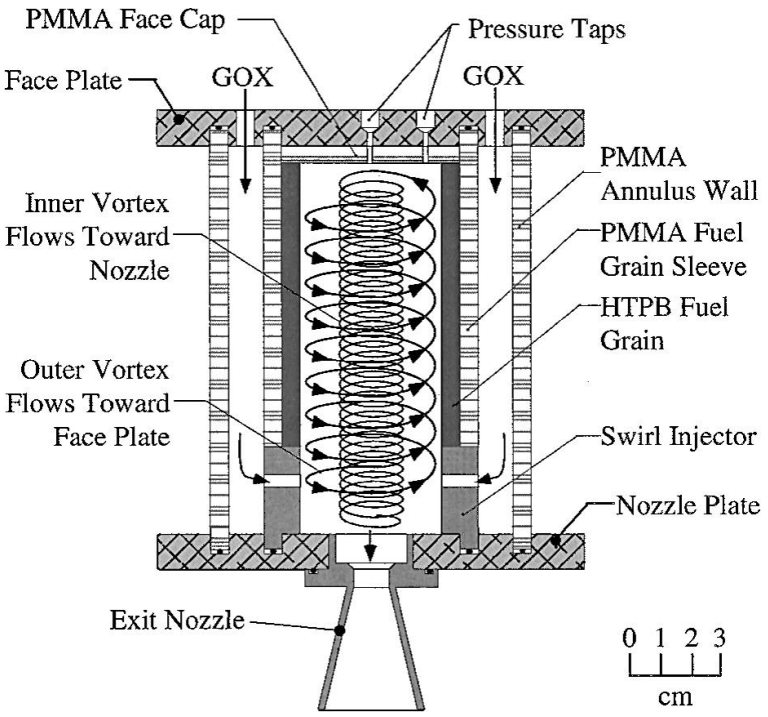

Figure 1.4. Schematic of a Vortex Injection Hybrid Rocket Engine (Knuth, Chiaverini, Sauer, & Gramer, 2002).

A lot of research and literature exists for the application of swirl injection of oxidizer into a hybrid rocket combustion chamber. The engine, termed as "Vortex Injection Hybrid Rocket Engine" is being developed and tested currently by Orbital Technologies Corporation. The literature, (Chiaverini & Kuo, 2007) gives a thorough description of the flowfield inside such a configuration. Figure 1.4 (Knuth, Chiaverini, Sauer, & Gramer, 2002) shows a schematic of the VIHRE. The oxidizer is injected

tangentially near the aft-end, forms a swirling counterflow inside the combustion chamber and exits through the nozzle. This considerably improves the residence time of the fuel-oxidizer mixture, along with improved mixing, efficiency, and a multi-fold increase in regression rate (Majdalani & Vyas, 2004).

The vortex injection concept has also been used for liquid rocket motors by Orbital Technologies. The cyclonic flow is used to keep the hot gases away from the chamber wall. The liquid oxygen is injected into the combustion chamber in such a way that it generates a stable, tornado-like cyclonic flow that confines the combustion to the central region of the chamber, which protects the surfaces. One such rocket was tested recently in the Mojave desert. The motor was a version of the 30,000-lb (13,600-kg) thrust liquid engine that Orbitec is developing for the U.S. Air Force"s Advanced Upper Stage Engine Program and for several NASA in-space and planetary propulsion systems including the Space Launch System. (Ashley, 2009)

Thus, swirling counterflows have a wide number of applications in the current and future industry and it is important to continue indepth research on this topic.

1.5 Organization of the thesis

This thesis is structured as follows: Chapter 2 gives the problem formulation and the analytical solution for the flowfield inside a cylindrical container in which fluid is tangentially injected. Chapter 3 deals with the setup, solution procedure and results for the 2D axisymmetric CFD problem. Chapter 4 gives the CFD setup and results for the full 3D case. A direct comparison between all the 3 cases: analytical,

2D axisymmetric CFD, and 3D axisymmetric CFD is also included in chapter 4. Chapter 5 gives the conclusion to this work.

2. Problem Formulation

The purpose of this section is to develop an analytical solution and plot the velocity profiles for a swirling flow which is developed when fluid is tangentially injected into a cylindrical container. The container is considered to be as follows (Figure 2.1).

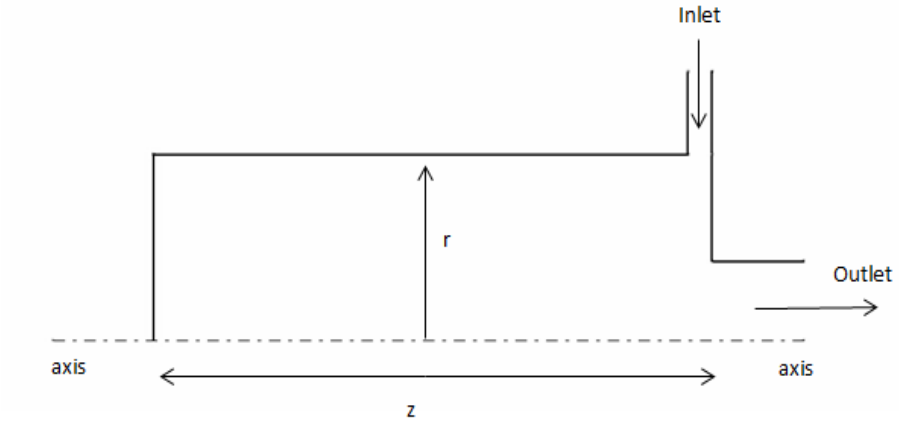

Figure 2.1. Schematic of the axisymmetric cylindrical container.

Fluid enters through the tangential inlet near the endwall that has the outlet. Due to the radial and axial pressure gradient developed(proved later), fluid is pushed out towards the wall and travels along the length of the container. As the fluid moves along the sidewall, the swirl decays due to viscous effects. These two effects lead to opposite axial pressure gradients near the axis and the sidewall, as well as opposite pressure gradients at the endwall near the inlet and away from the inlet. Thus, the

fluid travels axially along the sidewall, makes a U-turn at the dead-end, converges near the axis, and then travels back to the endwall with the outlet.

2.1 Solution Setup

The work done in this chapter is based upon the work done by (Shtern, 2012). However, the final equations that are derived and solved here are different from the ones used by (Shtern, 2012). Also, the boundary value problem solver 'bvp4c' in MATLAB is used to solve the equations numerically, instead of Newton's shooting method as done by (Shtern, 2012).

The assumptions made here are that the fluid is injected tangentially in a cylindrical container, the fluid being a viscous incompressible fluid. Starting with the unsteady incompressible Navier-Stokes equations in cylindrical coordinates, we have,

The $r-momentum$ equation

$$\frac{\partial v_r}{\partial t}+v_r\frac{\partial v_r}{\partial r}+\frac{v_\phi}{r}\frac{\partial v_r}{\partial \phi}+v_z\frac{\partial v_r}{\partial z}-\frac{v_\phi^2}{r}=-\frac{1}{\rho}\frac{\partial P}{\partial r}+\frac{\mu}{\rho}[\frac{\partial^2 v_r}{\partial r^2}+\frac{1}{r}\frac{\partial v_r}{\partial r}+\frac{1}{r^2}\frac{\partial^2 v_r}{\partial \phi^2}+\frac{\partial^2 v_r}{\partial z^2}-\frac{v_r}{r^2}-\frac{2}{r^2}\frac{\partial v_\phi}{\partial \phi}] \tag{2.1}$$

The $z-momentum$ equation

$$\frac{\partial v_z}{\partial t}+v_r\frac{\partial v_z}{\partial r}+\frac{v_\phi}{r}\frac{\partial v_z}{\partial \phi}+v_z\frac{\partial v_z}{\partial z}=-\frac{1}{\rho}\frac{\partial P}{\partial z}+\frac{\mu}{\rho}[\frac{\partial^2 v_z}{\partial r^2}+\frac{1}{r}\frac{\partial v_z}{\partial r}+\frac{1}{r^2}\frac{\partial^2 v_z}{\partial \phi^2}+\frac{\partial^2 v_z}{\partial z^2}] \tag{2.2}$$

The $\theta - momentum$ equation

$$\frac{\partial v_\phi}{\partial t} + v_r\frac{\partial v_\phi}{\partial r} + \frac{v_\phi}{r}\frac{\partial v_\phi}{\partial \phi} + v_z\frac{\partial v_\phi}{\partial z} + \frac{v_r v_\phi}{r} = -\frac{1}{\rho r}\frac{\partial P}{\partial \phi} + \frac{\mu}{\rho}[\frac{\partial^2 v_\phi}{\partial r^2} + \frac{1}{r}\frac{\partial v_\phi}{\partial r} + \frac{1}{r^2}\frac{\partial^2 v_\phi}{\partial \phi^2} + \frac{\partial^2 v_\phi}{\partial z^2} - \frac{v_\phi}{r^2} + \frac{2}{r^2}\frac{\partial v_r}{\partial \phi}] \tag{2.3}$$

The *continuity* equation

$$\frac{1}{r}\frac{\partial (r v_r)}{\partial r} + \frac{1}{r}\frac{\partial v_\phi}{\partial \phi} + \frac{\partial v_z}{\partial z} = 0 \tag{2.4}$$

Next, the Navier-Stokes equations are non dimensionalized using the following scales

1. Length scale -R_{in} , the cylindrical container's inner radius.
2. Velocity scale - $v_{\phi sc}$, the characteristic swirl velocity.
3. Pressure scale - $\rho v_{\phi sc}^2$, where ρ is the density of the fluid.

Also, applying the assumptions that the flow is steady and axisymmetric, equations (2.1), (2.2), (2.3), and (2.4) reduce to the following equations

$$v_r\frac{\partial v_r}{\partial r} + v_z\frac{\partial v_r}{\partial z} - \frac{v_\phi^2}{r} + \frac{\partial P}{\partial r} = \frac{1}{Re}[\frac{1}{r}\frac{\partial}{\partial r}(r\frac{\partial v_r}{\partial r}) - \frac{v_r}{r^2} + \frac{\partial^2 v_r}{\partial z^2}] \tag{2.5}$$

$$v_r\frac{\partial v_z}{\partial r} + v_z\frac{\partial v_z}{\partial z} + \frac{\partial P}{\partial z} = \frac{1}{Re}[\frac{1}{r}\frac{\partial}{\partial r}(r\frac{\partial v_z}{\partial r}) + \frac{\partial^2 v_z}{\partial z^2}] \tag{2.6}$$

$$v_r \frac{\partial v_\phi}{\partial r} + \frac{v_r v_\phi}{r} + v_z \frac{\partial v_\phi}{\partial z} = \frac{1}{Re}[\frac{\partial^2 v_\phi}{\partial r^2} + \frac{1}{r}\frac{\partial v_\phi}{\partial r} - \frac{v_\phi}{r^2} + \frac{\partial^2 v_\phi}{\partial z^2}] \tag{2.7}$$

$$\frac{\partial (r v_r)}{\partial r} + \frac{\partial (r v_z)}{\partial z} = 0 \tag{2.8}$$

Where $Re = v_{\phi sc} R_{in}/\nu$ is the Reynolds number, and ν is the kinematic viscosity. The Stream function ψ is introduced in the above equations by substituting v_r and v_z as follows

$$v_r = -\frac{1}{r}\frac{\partial \psi}{\partial z} \tag{2.9}$$

$$v_z = \frac{1}{r}\frac{\partial \psi}{\partial r} \tag{2.10}$$

where ψ is scaled by $2\pi R_{in}^2 \rho v_{\phi sc}$

This satisfies the continuity equation (eqn (2.8))

The next step is to eliminate the pressure gradients $\partial P/\partial r$ and $\partial P/\partial z$. This is done by substituting ψ from equations (2.9) and (2.10) into (2.5) and (2.6). Then these reduced r and z momentum equations are differentiated w.r.t z and r respectively. A common term $\partial^2 P/\partial r \partial z$ is obtained in both the equations, which is eliminated by substituting one equation in the other.

Substituting equations (2.9) and (2.10) in equation (2.5), we get

$$-\frac{1}{r}\frac{\partial\psi}{\partial z}\frac{\partial}{\partial r}(-\frac{1}{r}\frac{\partial\psi}{\partial z})+\frac{1}{r}\frac{\partial\psi}{\partial r}\frac{\partial}{\partial z}(-\frac{1}{r}\frac{\partial\psi}{\partial z})-\frac{v_{\phi^2}}{r}+\frac{\partial P}{\partial r}= \\ \frac{1}{Re}[\frac{1}{r}\frac{\partial}{\partial r}\{r\frac{\partial}{\partial r}(-\frac{1}{r}\frac{\partial\psi}{\partial z})\}-\frac{1}{r^2}(-\frac{1}{r}\frac{\partial\psi}{\partial z})+\frac{\partial^2}{\partial z^2}-\frac{1}{r}\frac{\partial\psi}{\partial z}] \tag{2.11}$$

Simplifying

$$\frac{1}{r}\frac{\partial\psi}{\partial z}\frac{\partial}{\partial r}(\frac{1}{r}\frac{\partial\psi}{\partial z})-\frac{1}{r^2}\frac{\partial\psi}{\partial r}\frac{\partial^2\psi}{\partial z^2}-\frac{v_{\phi^2}}{r}+\frac{\partial P}{\partial r}= \\ \frac{1}{Re}[-\frac{1}{r}\frac{\partial}{\partial r}\{r\frac{\partial}{\partial r}(\frac{1}{r}\frac{\partial\psi}{\partial z})\}+\frac{1}{r^3}\frac{\partial\psi}{\partial z}-\frac{1}{r}\frac{\partial^3\psi}{\partial z^2\partial r}]$$

Differentiating this equation by z, we get

$$Re\frac{\partial}{\partial z}[\frac{1}{r}\frac{\partial\psi}{\partial z}\frac{\partial}{\partial r}(\frac{1}{r}\frac{\partial\psi}{\partial z})-\frac{1}{r^2}\frac{\partial\psi}{\partial r}\frac{\partial^2\psi}{\partial z^2}-\frac{v_{\phi^2}}{r}]+Re\frac{\partial^2 P}{\partial r\partial z}= \\ -\frac{1}{r}\frac{\partial^2}{\partial r\partial z}\{r\frac{\partial}{\partial r}(\frac{1}{r}\frac{\partial\psi}{\partial z})\}+\frac{1}{r^3}\frac{\partial^2\psi}{\partial z^2}-\frac{1}{r}\frac{\partial^4\psi}{\partial z^3\partial r}]$$

Rearranging,

$$Re\frac{\partial^2 P}{\partial r\partial z}=-Re\frac{\partial}{\partial z}[\frac{1}{r}\frac{\partial\psi}{\partial z}\frac{\partial}{\partial r}(\frac{1}{r}\frac{\partial\psi}{\partial z})-\frac{1}{r^2}\frac{\partial\psi}{\partial r}\frac{\partial^2\psi}{\partial z^2}-\frac{v_{\phi^2}}{r}] \\ -\frac{1}{r}\frac{\partial^2}{\partial r\partial z}\{r\frac{\partial}{\partial r}(\frac{1}{r}\frac{\partial\psi}{\partial z})\}+\frac{1}{r^3}\frac{\partial^2\psi}{\partial z^2}-\frac{1}{r}\frac{\partial^4\psi}{\partial z^3\partial r}] \tag{2.12}$$

Substituting eqns (9) and (10) in eqn (6), we get

$$(-\frac{1}{r}\frac{\partial\psi}{\partial z})\frac{\partial}{\partial r}(\frac{1}{r}\frac{\partial\psi}{\partial r})+(\frac{1}{r}\frac{\partial\psi}{\partial r})\frac{\partial}{\partial z}(\frac{1}{r}\frac{\partial\psi}{\partial r})+\frac{\partial P}{\partial z}= \\ \frac{1}{Re}[\frac{1}{r}\frac{\partial}{\partial r}\{r\frac{\partial}{\partial r}(\frac{1}{r}\frac{\partial\psi}{\partial r})\}+\frac{\partial^2}{\partial z^2}(\frac{1}{r}\frac{\partial\psi}{\partial r})]$$

Simplifying,

$$-\frac{1}{r}\frac{\partial\psi}{\partial z}\frac{\partial}{\partial r}(\frac{1}{r}\frac{\partial\psi}{\partial r})+\frac{1}{r^2}\frac{\partial\psi}{\partial r}\frac{\partial^2\psi}{\partial r\partial z})+\frac{\partial P}{\partial z}=\frac{1}{Re}[\frac{1}{r}\frac{\partial}{\partial r}\{r\frac{\partial}{\partial r}(\frac{1}{r}\frac{\partial\psi}{\partial r})\}+\frac{\partial^2}{\partial z^2}(\frac{1}{r}\frac{\partial\psi}{\partial r})]$$

Differentiating the above equation by r, we get

$$\begin{aligned}Re\frac{\partial}{\partial r}[-\frac{1}{r}\frac{\partial\psi}{\partial z}\frac{\partial}{\partial r}(\frac{1}{r}\frac{\partial\psi}{\partial r})+\frac{1}{r^2}\frac{\partial\psi}{\partial r}\frac{\partial^2\psi}{\partial r\partial z})]+Re\frac{\partial^2 P}{\partial r\partial z}=\\ \frac{\partial}{\partial r}[\frac{1}{r}\frac{\partial}{\partial r}\{r\frac{\partial}{\partial r}(\frac{1}{r}\frac{\partial\psi}{\partial r})\}]+\frac{\partial^3}{\partial z^2\partial r}(\frac{1}{r}\frac{\partial\psi}{\partial r})\end{aligned} \tag{2.13}$$

Substituting the value of $Re\frac{\partial^2 P}{\partial r\partial z}$ from equation (12) into equation (13), we get

$$\begin{aligned}\frac{\partial}{\partial r}\left\{\frac{1}{r}\frac{\partial}{\partial r}\left[r\frac{\partial}{\partial r}\left(\frac{1}{r}\frac{\partial\psi}{\partial r}\right)\right]\right\}+\frac{\partial^3}{\partial z^2\partial r}\left[\frac{1}{r}\frac{\partial\psi}{\partial r}\right]+\frac{1}{r}\frac{\partial^2}{\partial r\partial z}\left[r\frac{\partial}{\partial r}\left(\frac{1}{r}\frac{\partial\psi}{\partial z}\right)\right]-\frac{1}{r^3}\frac{\partial^2\psi}{\partial z^2}+\frac{1}{r}\frac{\partial^4\psi}{\partial z^4}=\\ Re\frac{\partial}{\partial r}\left[\frac{1}{r^2}\frac{\partial\psi}{\partial r}\frac{\partial^2\psi}{\partial r\partial z}-\frac{1}{r}\frac{\partial\psi}{\partial z}\frac{\partial}{\partial r}\left(\frac{1}{r}\frac{\partial\psi}{\partial r}\right)\right]+Re\frac{\partial}{\partial z}[\frac{1}{r}v_\phi^2-\frac{1}{r}\frac{\partial\psi}{\partial z}\frac{\partial}{\partial r}(\frac{1}{r}\frac{\partial\psi}{\partial z})+\frac{1}{r^2}\frac{\partial\psi}{\partial r}\frac{\partial^2\psi}{\partial z^2}]\end{aligned} \tag{2.14}$$

Substituting eqns (9) and (10) in eqn eqn(7)

$$-\frac{1}{r}\frac{\partial\psi}{\partial z}\frac{\partial v_\phi}{\partial r}-\frac{1}{r}\frac{\partial\psi}{\partial z}\frac{v_\phi}{r}+\frac{1}{r}\frac{\partial\psi}{\partial r}\frac{\partial v_\phi}{\partial z}=\frac{1}{Re}[\frac{\partial^2 v_\phi}{\partial r^2}+\frac{1}{r}\frac{\partial v_\phi}{\partial r}-\frac{v_\phi}{r^2}+\frac{\partial^2 v_\phi}{\partial z^2}]$$

Rearranging,

$$\frac{\partial^2 v_\phi}{\partial r^2} + \frac{1}{r}\frac{\partial v_\phi}{\partial r} - \frac{v_\phi}{r^2} + \frac{\partial^2 v_\phi}{\partial z^2} = Re\left[\frac{1}{r}\frac{\partial \psi}{\partial r}\frac{\partial v_\phi}{\partial z} - \frac{1}{r}\frac{\partial \psi}{\partial z}\left(\frac{\partial v_\phi}{\partial r} + \frac{v_\phi}{r}\right)\right] \tag{2.15}$$

Thus, The pressure terms are eliminated completely and the four equations started with are reduced to just two equations (2.14) and (2.15)

2.2 Swirl Decay

The flow in the core region(away from the end walls) is considered. This flow is assumed to have very weak dependence in the z-direction.

The swirling flow decays from the inlet to the outlet as the fluid is viscous and no slip boundary conditions are applied to the wall. To model this decay, the solution is assumed to be in the form of

$$v_\phi = F(r)e^{-\lambda z} + O(\lambda^2) \tag{2.16}$$

and

$$\psi = Q(r)e^{-\lambda z} + O(\lambda^2) \tag{2.17}$$

λ is assumed to be the decay rate in the z-direction. As the flow is assumed to have a very weak dependence in the z-direction, $\lambda << 1$

Also, as the swirl is strong, $Re >> 1$. Hence the product of λRe cannot be neglected.

Therefore, substituting eqns (2.16) and (2.17) in (2.14), fulfilling differentiation by z and setting $\lambda = 0$ everywhere, while still retaining the λRe terms, we get

$$\frac{\partial}{\partial r}\left\{\frac{1}{r}\frac{\partial}{\partial r}\left[r\frac{\partial}{\partial r}\left(\frac{1}{r}Q'e^{-\lambda z}\right)\right]\right\} =$$
$$Re\frac{\partial}{\partial r}\left[\frac{1}{r^2}Q'e^{-\lambda z}(-\lambda)Q'e^{-\lambda z} - \frac{1}{r}(-\lambda)Qe^{-\lambda z}\frac{\partial}{\partial r}\left(\frac{1}{r}Q'e^{-\lambda z}\right)\right] + \frac{Re}{r}\frac{\partial}{\partial z}(F^2e^{-2\lambda z})]$$

Simplifying,

$$\left\{\frac{1}{r}\left[r\left(\frac{1}{r}Q'\right)'\right]'\right\}' = \lambda Re\{[\frac{1}{r}Q(\frac{1}{r}Q')' - \frac{1}{r^2}Q'^2]' - \frac{2}{r}F^2\} \tag{2.18}$$

Substituting (2.16) and (2.17) into (2.15),

$$\frac{\partial^2(Fe^{-\lambda z})}{\partial r^2} + \frac{1}{r}\frac{\partial(Fe^{-\lambda z})}{\partial r} - \frac{(Fe^{-\lambda z})}{r^2} + \frac{\partial^2(Fe^{-\lambda z})}{\partial z^2} =$$
$$Re\left[\frac{1}{r}\frac{\partial}{\partial r}(Qe^{\lambda z})\frac{\partial}{\partial z}Fe^{-\lambda z}) - \frac{1}{r}\frac{\partial}{\partial z}(Qe^{-\lambda z})\left(\frac{\partial}{\partial r}(Fe^{-\lambda z}) + \frac{(Fe^{-\lambda z})}{r}\right)\right]$$

Simplifying,

$$F'' + \frac{F'}{r} - \frac{F}{r^2} = \lambda Re\left[\frac{Q}{r}\left(F' + \frac{F}{r}\right) - \frac{Q'F}{r}\right] \tag{2.19}$$

Again, pointing out that F is the tangential velocity and Q is the stream function, ψ, we define the axial velocity as $W = Q'/r$. Since the axis is a streamline, $\psi =$ *constant*, putting $Q = 0$ at the axis $r = 0$, and also applying the no slip boundary condition at the side wall, $r = 1$, we end up with these boundary conditions,

$$Q(0) = Q'(0) = 0 \tag{2.20}$$

$$Q(1) = Q'(1) = 0 \tag{2.21}$$

$$F(0) = 0 \tag{2.22}$$

$$F(1) = 0 \tag{2.23}$$

This boundary value problem has a trivial solution. In order to obtain a non-zero solution, an eigen value, which is λRe in this case, must be found.

The above boundary value problem is rewritten as a system of first order differential equations as follows.

$$F' = F_1 \tag{2.24}$$

$$F_1' = \frac{F}{r^2} - \frac{F_1}{r} + \lambda Re\left(\frac{QF_1}{r} + \frac{QF}{r^2} - WF\right) \tag{2.25}$$

$$Q' = rW \tag{2.26}$$

$$W' = W_1/r \tag{2.27}$$

$$W_1' = rW_2 \tag{2.28}$$

Substituting these values into equation (18)

$$\left\{\frac{1}{r}\left[rW'\right]'\right\}' = \lambda Re\{[\frac{1}{r}QW' - W^2]' - \frac{2}{r}F^2\}$$

$$\left\{\frac{1}{r}W_1'\right\}' = \lambda Re\{[\frac{1}{r^2}QW_1 - W^2]' - \frac{2}{r}F^2\}$$

$$W_2' = \lambda Re\{[-\frac{2}{r^3}QW_1 + \frac{1}{r^2}Q'W_1 + \frac{1}{r^2}QW_1' - 2WW' - \frac{2}{r}F^2\}$$

$$W_2' = \lambda Re\frac{\left(QW_2 - \frac{2QW_1}{r^2} - WW_1 - 2F^2\right)}{r} \tag{2.29}$$

2.3 Matlab Simulation

The boundary value problem to be solved now consists of the following equations,

$$F' = F_1 \tag{2.30}$$

$$F_1' = \frac{F}{r^2} - \frac{F_1}{r} + \lambda Re\left(\frac{QF_1}{r} + \frac{QF}{r^2} - WF\right) \tag{2.31}$$

$$Q' = rW \tag{2.32}$$

$$W' = W_1/r \tag{2.33}$$

$$W_1' = rW_2 \tag{2.34}$$

$$W_2' = \lambda Re \frac{\left(QW_2 - \frac{2QW_1}{r^2} - WW_1 - 2F^2\right)}{r} \tag{2.35}$$

The boundary conditions are set as

$$Q(0) = Q'(0) = 0 \tag{2.36}$$

$$Q(1) = Q'(1) = 0 \tag{2.37}$$

$$F(0) = 0 \tag{2.38}$$

$$F(1) = 0 \tag{2.39}$$

$$F_1(0) = 0 \tag{2.40}$$

To compute the proper eigen value, MATLAB requires an extra boundary condition that excludes the zero solution. This extra condition is provided by equation(2.40), which is $F_1(0) = 0$. (Shtern, 2012)

The boundary value problem is solved using MATLAB's 'bvp4c' solver. This solver uses collocation method to solve the ordinary differential equations.

'bvp4c' requires an initial guess for the desired solution. The initial solution is guessed on the basis of behaviour of different velocity profiles(Shtern, 2012) as follows :

$$F = r \tag{2.41}$$

$$F' = 1 \tag{2.42}$$

$$Q = 4r - 4r^2 \tag{2.43}$$

$$W = -0.246991(4r^2 - 3r^4 - 1) \tag{2.44}$$

$$W' = 8r^2 - 12r^4 \tag{2.45}$$

$$W_2 = 5.7242\cos(3r) \tag{2.46}$$

To compute the proper eigen value, MATLAB requires an extra boundary condition that excludes the zero solution. This extra condition is provided by equation(2.40), which is $F_1(0) = 0$.

bvp4c also requires an initial guess for the eigen-value. The better the guess, the faster the solution will converge. The guess here is set to 319.15. (Shtern, 2012)

The solution is calculated in 3 steps with different number of mesh points and relative tolerances. The solution for each step acts as the initial guess for the next step.

2.4 Velocity Profiles

Figure 2.2 represents the radial distribution of the tangential or the swirl velocity. The x-axis represents the non-dimensional radial distance from the axis, 0 being the axis and 1 being the sidewall. The swirl velocity increases from 0 away from the axis, reaches a certain maxiumum value, and then falls back to zero as it goes towards the sidewall.

The plot for F' is plotted just to verify whether the solution behaves correctly. As F' is the derivative of F, the plot from F' behaves as the plot for the slope of F

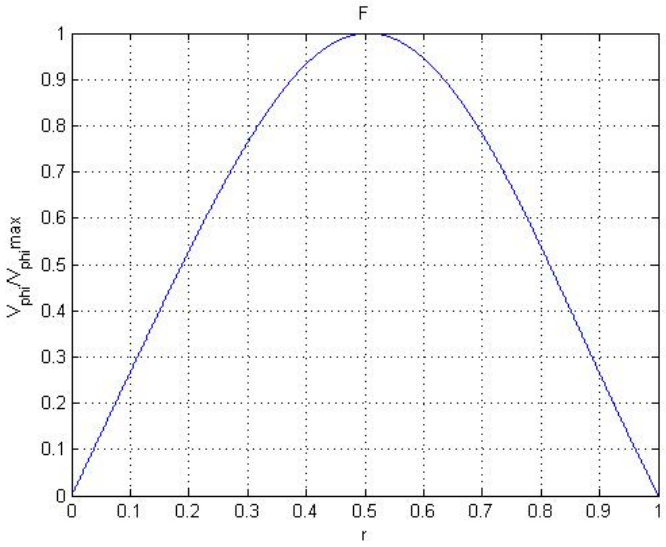

Figure 2.2. Tangential velocity.

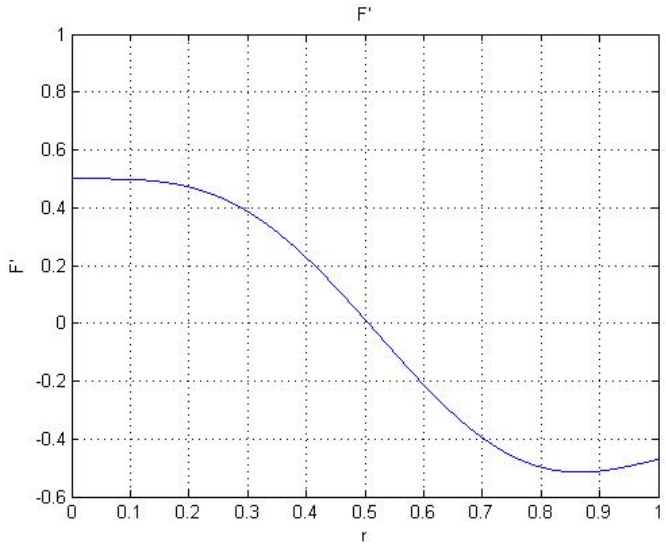

Figure 2.3. plot for F'(to validate the correct behaviour of the solution)

would, constant slope at the beginning, decreases to 0 as it reaches the maxima, and then becomes negative after the maxima.

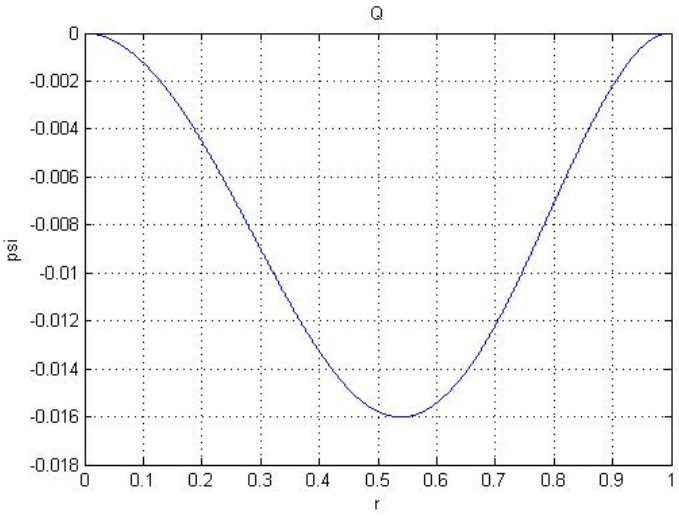

Figure 2.4. Streamfunction(mass flow rate).

Figure 2.4 represents the mass flow rate (ψ normalized by $2\pi R_{in}\rho v_{\phi sc}$). ψ first decreases away from the axis, reaches its minimum value where the axial velocity changes its direction, then goes back to zero at the sidewall.

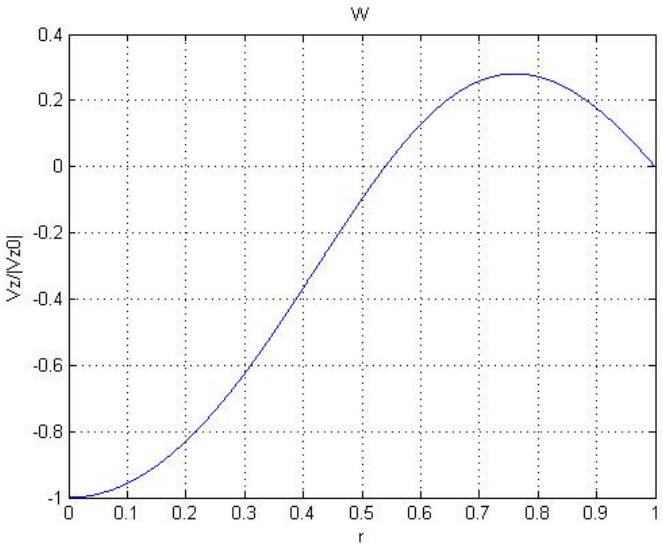

Figure 2.5. Axial Velocity.

Figure 2.5 represents the axial velocity scaled by the absolute value at the axis $|V_{z0}|$. The positive axial velocity represents the flow towards the dead end while the negative axial velocity represents the flow towards the exhaust. The axial velocity changes its sign at about $r = 0.53$, the same value as where the mass flow rate is the maximum. The maximum value of axial velocity is about 0.28, at $r = 0.76$. The opposite directions of the axial velocity validates the counterflow in the container.

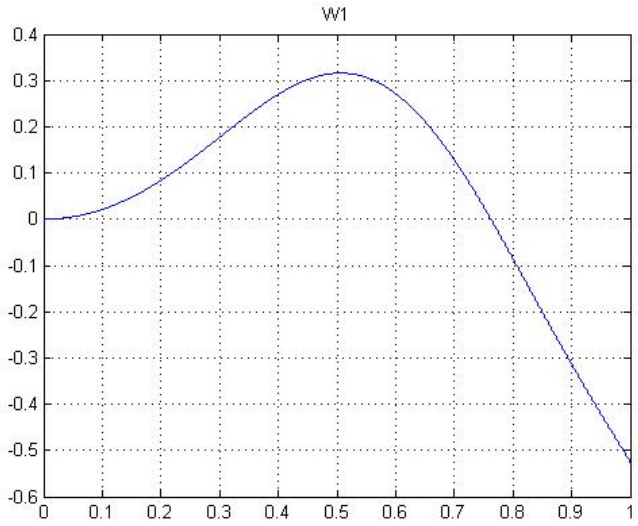

Figure 2.6. plot for W'(to validate the correct behaviour of the solution).

The plot for W1 (fig 2.6) is again, to validate that the solution is behaving correctly, as it is the plot for the slope of W.

The plot for W2(fig 2.7) relates to the pressure distribution of the solution as is shown below.

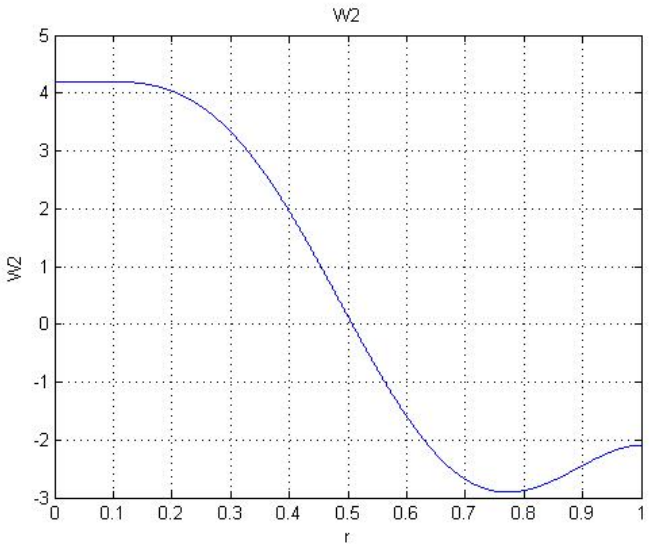

Figure 2.7. W2 relates to pressure distribution.

2.5 Pressure Distribution

Considering that the radial velocity v_r is negligible in the core flow, the equation (2.5) can be reduced to the cyclostrophic balance equation (Shtern, 2012),

$$\frac{\partial p}{\partial r} = \frac{v_\phi^2}{r} \tag{2.47}$$

Since v_ϕ^2/r is always greater than 0, the radial pressure gradient is always positive at any z. This causes the fluid to push towards the wall when it is injected into the container.

Integrating the above equation gives

$$p = p_0(z) + \int_0^r r^{-1} v_\phi^2 dr \tag{2.48}$$

where $p_0(z)$ is the pressure at the axis, $r = 0$.

Also, equation (2.6) reduces to

$$\frac{\partial p}{\partial z} = \frac{1}{Re}[W_2 + \lambda Re(W^2 - \frac{1}{r^2}W_1 Q)] \tag{2.49}$$

At the sidewall, $r = 1$, $Q(1) = 0$, $W(1) = 0$ (since $Q'(1) = 0$ and $W = Q'/r$)

Therefore the equation (2.49) reduces to

$$\frac{\partial p}{\partial z} = \frac{1}{Re}W_2(1) \tag{2.50}$$

From figure 2.7, it can be seen that $W_2(1) < 0$. Hence, $\partial p/\partial z < 0$ at $r = 1$. This negative pressure gradient pushes the fluid towards the deadend along the sidewall.

At $r = 0$, the equation (2.49) again reduces to

$$\frac{\partial p}{\partial z} = \frac{1}{Re}W_2(0) \tag{2.51}$$

From figure "2.7", $W_2(0) > 0$. Hence, pressure decreases from the dead end to the outlet along the axis, which pushes the flow towards the outlet near the axis, $r = 0$.

3. 2D Axisymmetric CFD of Swirling Flow in a Confined Cylinder with Endwall Rotation

In this chapter, the solution of the swirling counterflow is obtained by using CFD. The results obtained are compared with the similarity analysis performed in the previous chapter.

The flow inside a confined cylinder with endwall rotation is one of the simplest model and most fundamental one to analyse swirling flows. The steady-state flow produced in a closed cylindrical container by rotation of one endwall is determined by the aspect ratio H/R and Reynolds number $\omega R^2/\nu$, H being the cylinder length, R its radius, ω the angular velocity of the endwall, and ν the kinematic viscosity of the contained fluid. The rotating endwall acts as a pump, drawing in fluid axially and driving it away in an upward spiral. In a closed container, the fluid swirls along the cylindrical wall. Spirals in across the fixed endwall and then again turns into the axial direction towards the rotating endwall. The inward spiraling motion results in an initial increase in swirl velocity, due to the conservation of angular momentum, and so the creation of a concentrated vortex.

When this experiment was first conducted, it was observed that for certain Reynolds numbers and H/R ratio, the vortex underwent breakdown, i.e a stagnation point followed by a recirculation zone of limited extent appears on the cylinder axis. Vortex

breakdowns are desirable in some cases while are undesirable in many others. For example, it is important to breakdown the trailing vortices from a large aircraft wings such that it does not affect smaller aircrafts flying in its wake. However, leading-edge vortices shed from a delta wing induce a velocity field that results in increased lift and stability of the wing.

3.1 Physical Model

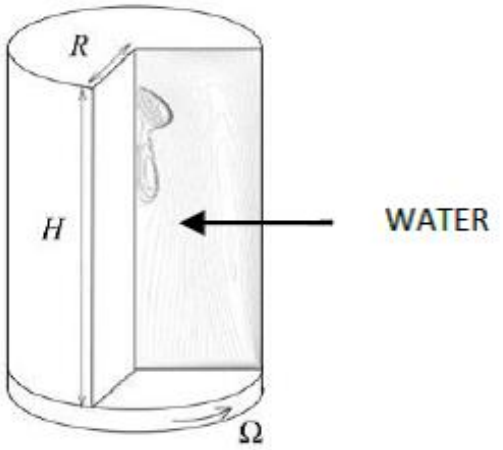

Figure 3.1. Cylinder filled with water and rotating base.

As no slip conditions are applied to all the walls, the viscous fluid will start to move along with the rotating wall and due to centrifugal force, will be pushed out to the outside of the cylinder(figure 3.1 (Lopez, 2012)). With the base rotating continuously, more and more fluid is pushed to the outer wall and the fluid already there is pushed up along the surface. This fluid, after reaching the head of the cylinder, is deflected towards the axial direction, from where it moves down again towards the base. As

the fluid reaches the base, the process is again repeated and after some time, the flow reaches a steady state. The flow is stable for low Reynolds number. But as the Reynolds number begins to increase, the flow becomes more and more turbulent. After a certain critical Reynolds number, a vortex breakdown is observed near the head wall along the axial direction.

3.2 Mesh

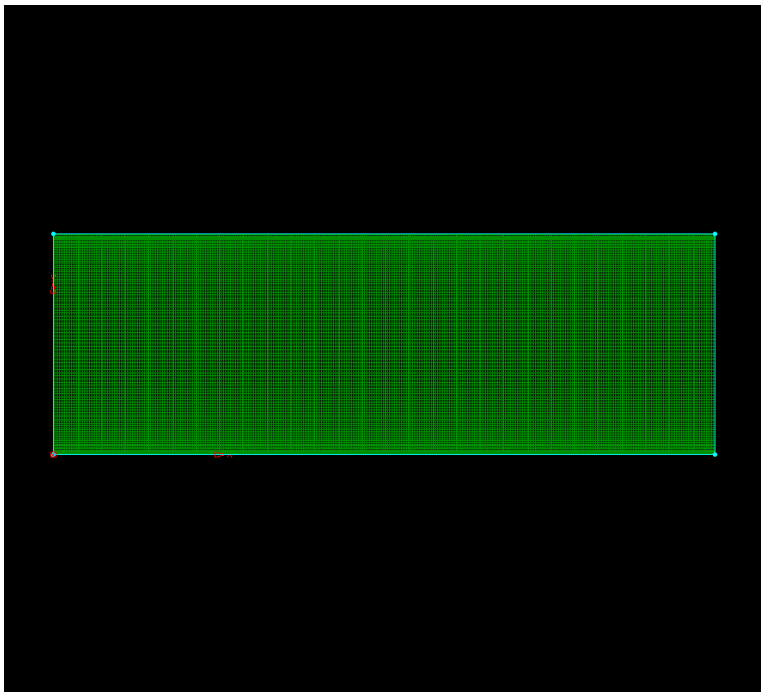

Figure 3.2. Structured mesh for the 2D Axisymmetric CFD simulation

Pointwise is used for creating the mesh for this simulation. A simple rectangle is used as the geometry to represent the axisymmetric cross-section of the cylinder. The bottom side of the rectangle is the axis of the cylinder. The left side denotes the

rotating end-wall. The top side is the sidewall, and the right side is the stationary endwall. The structured grid has 400 divisions horizontally, and 100 divisions vertically. The mesh is refined near the sidewall and the axis to appropriately capture the wall effects and vortex breakdown(if any) near the axis of the cylinder. The total number of points for the mesh is 40,000. A grid independent study was done and it was found that there was no noticeable difference in the solution beyond 40,000 points.

The sides of the rectangle are referred to as left, right , bottom, and top henceforth. The boundary conditions applied are as follows

- **Left** - Rotating Wall boundary condition with no-slip. The angular velocity is set to 1 rad/s.
- **Right** - Stationary Wall boundary condition with no-slip.
- **Bottom** - Axis boundary condition.
- **Top** - Stationary Wall boundary condition with no slip.

3.3 Numerical Setup

The solution is obtained using the commercially available software Ansys-Fluent. Fluent uses finite volume method to simulate flowfields.

As the flow is a very highly swirling flow, turbulence and swirl effects have to be taken into consideration. The turbulence model used to solve for this flow is the RNG(Re-normalization group) $k-\epsilon$ model with Swirl enhanced flows. The RNG $k-\epsilon$ model has an additional ϵ term in its equation that significantly improves the accuracy for rapidly strained flows. The swirling effect on turbulence is included in the RNG model, which considerably improves the accuracy for swirling flows.(Itai, Ferreira, Guerra, & Mesquita, 2006)

For pressure discretization, the default scheme in FLUENT interpolates the pressure values at the faces using momentum equation coefficients. This procedure is good when there is smooth pressure variation between cell centers. When jumps or large gradients in the momentum source terms between control volumes, the pressure profile has a high gradient at the cell face, and this scheme interpolates it with poor accuracy. If this scheme is used, the discrepancy shows up in overshoots/undershoots of cell velocity. Swirling flows have large fluctuations in their velocities. In such cases, it is necessary to pack the mesh in regions of high gradient to resolve the pressure variation adequately. Another source of error is that FLUENT assumes that the normal pressure gradient at the wall is zero. This is valid for boundary layers, but not in the presence of body forces or curvature. Again, the failure to correctly

account for the wall pressure gradient is manifested in velocity vectors pointing in-/out of walls. Several alternate methods are available for cases in which the standard pressure interpolation scheme is not valid. One of them is the PRESTO! Pressure discretization scheme. The PRESTO! (PREssure STaggering Option) scheme uses the discrete continuity balance for a "staggered" control volume about the face to compute the "staggered" (i.e. face) pressure. This procedure is similar in spirit to the staggered-grid schemes used with structured meshes.

3.4 Results

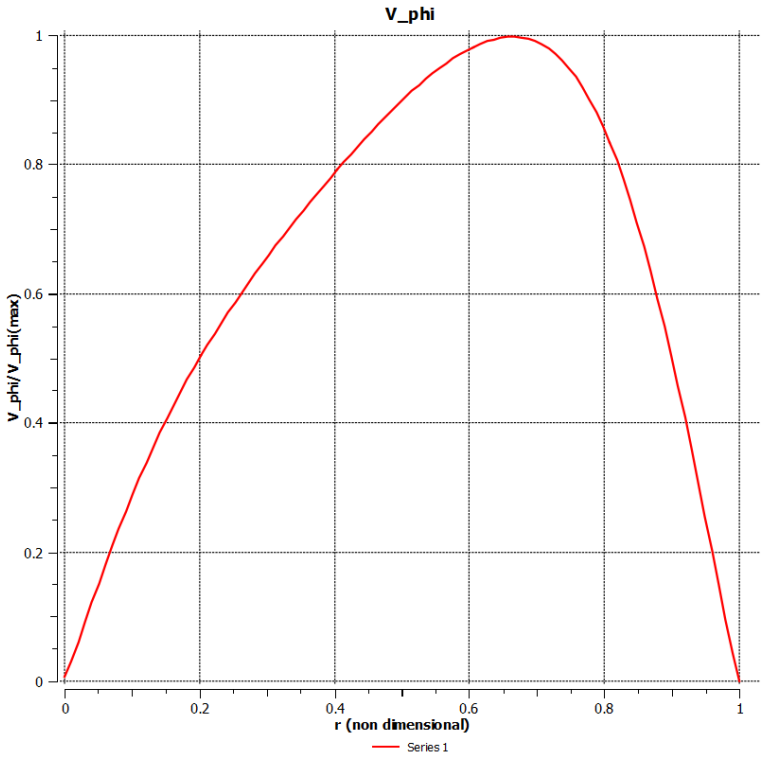

Figure 3.3. Tangential Velocity profile

Figure 3.3 shows the tangential velocity profile for the two dimensional CFD simulation. The solution behaves as was found out in the analytical solution. The swirl velocity starts increasing from zero away from the axis, reaches a maximum value, and then falls back down to zero near the sidewall. However, the peak for this velocity is shifted towards the sidewall, as opposed the maximum value attained exactly at $r = 0.5$ in the analytical solution.

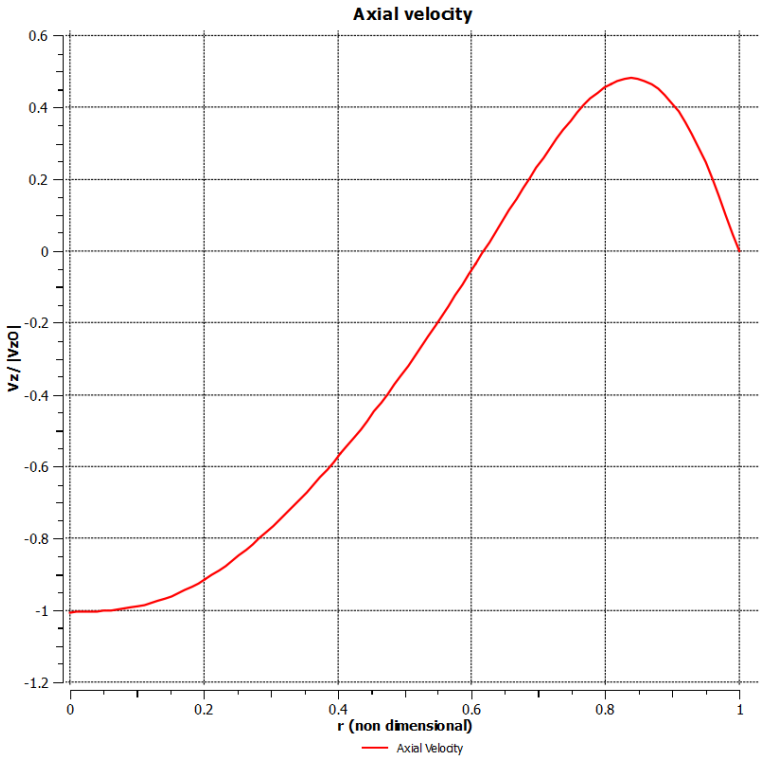

Figure 3.4. Axial Velocity

Figure 3.4 shows the plot for the axial velocity scaled to its absolute value at $r = 0$. This plot behaves exactly the same way as for the analytical solution. The positive axial velocity corresponds to the flow near the sidewall moving towards the

dead-end whereas the negative axial velocity represents the flow near the axis which is traveling towards the exhaust.

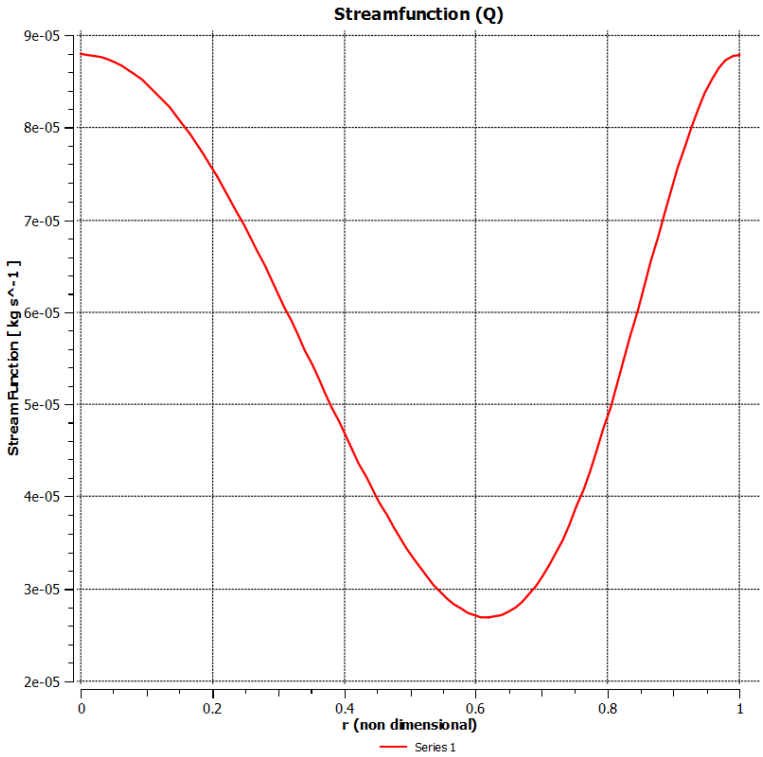

Figure 3.5. Streamfunction (mass flow rate)

The plot in Figure 3.5 shows the mass flow rate from the axis to the sidewall. Once again, it can be seen that the mass flow rate reaches its peak at the same spot as the axial velocity changes its direction.

4. 3D Simulation of a Swirling Counterflow

In this section, a 3D model of a swirling counterflow in a cylindrical chamber is created. Fluid is injected through a tangential inlet near the aft-end. The physics of the problem remain the same as the previous two cases. The results for the 3D simulation are compared with the analytical solution and the 2D axisymmetric solution.

4.1 Geometry

The geometry was created using Catia V5. The H/R ratio was chosen to be 6.

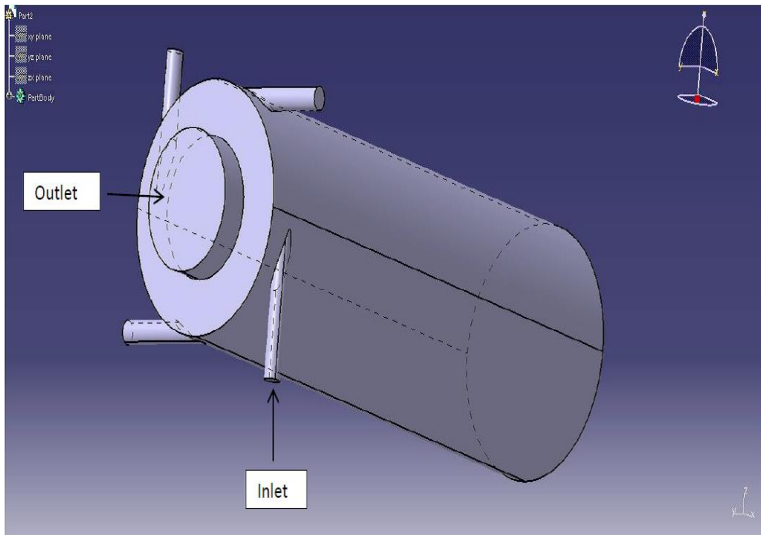

Figure 4.1. Geometry for the 3D CFD simulation with 4 inlets.

Initially, 4 tangential inlets were used in the geometry to inject the fluid into the cylindrical chamber, as shown in the figure. However, when the simulation was ran,

the results were not consistent with the analytical and the 2D axisymmetric solutions. The velocity vectors and the streamlines showed a lot of turbulence and mixing near the inlets as the flows converged which affected the solution throughout.

Hence, a single inlet was chosen for the final simulation which provided with results much similar to the previous two cases.

The configuration remains the same as previous, fluid is injected tangentially near the end-wall that has the outlet, while the other end-wall remains closed.

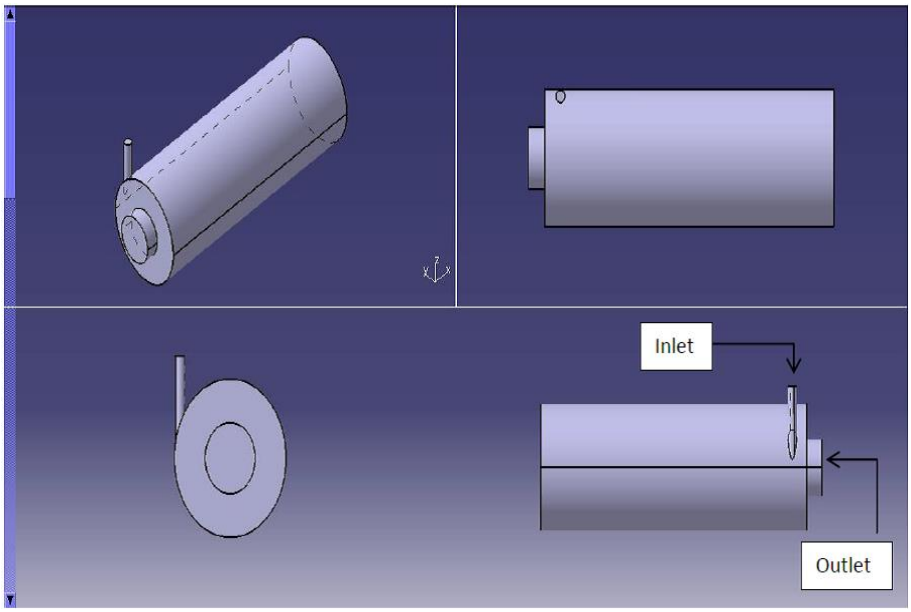

Figure 4.2. Modified Geometry for the 3D CFD simulation with one inlet.

4.2 Mesh

The mesh was generated using Pointwise. It is an unstructured tetrahedral mesh. The total number of cells is 2,463,835. A grid independent study was done on this

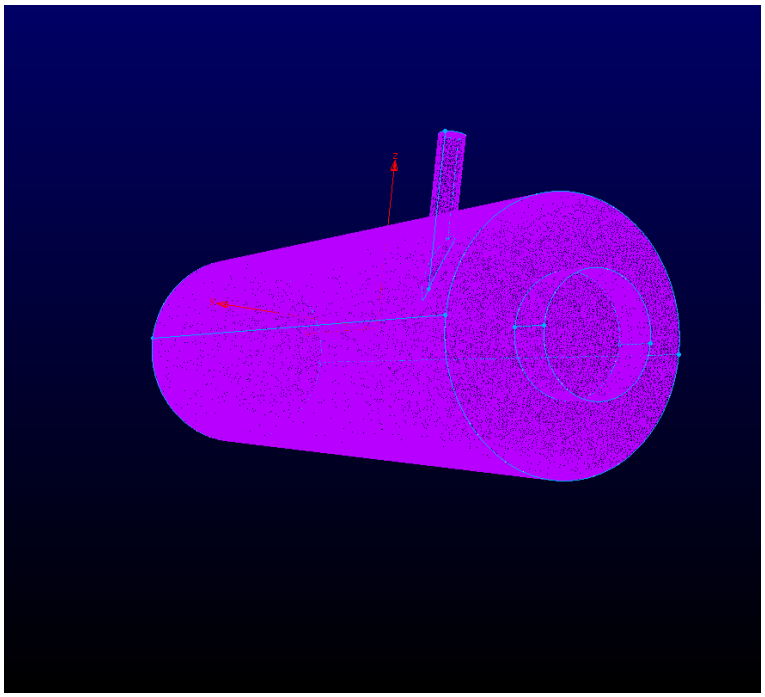

Figure 4.3. Mesh for the 3D case.

case and a more refined mesh than the above number of cells had no considerable effect on the solution.

4.3 Boundary Conditions

Velocity Inlet boundary condition is applied to the inlet shown in fig 4.2. Pressure Outlet boundary condition is applied to the outlet as shown in fig 4.2. Every other surface has a Wall boundary condition with no-slip. The velocity is set such the Reynolds number for the case is 2000.

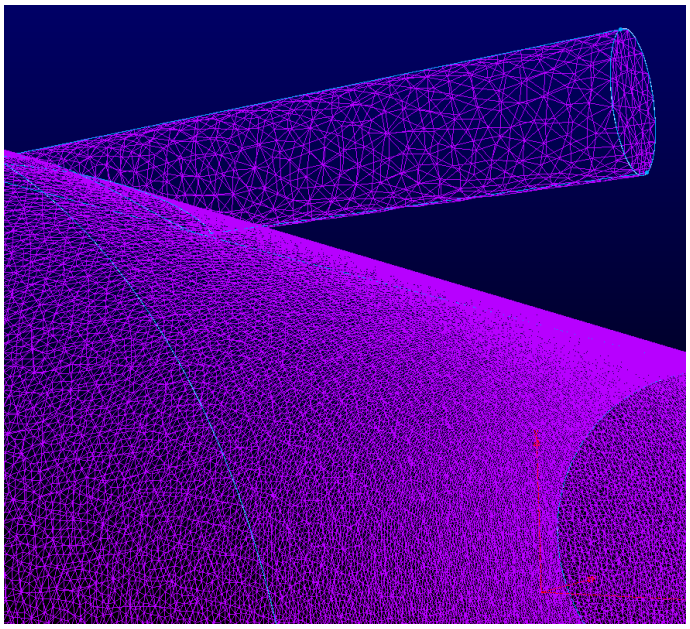

Figure 4.4. Unstructured mesh for the 3D setup(zoomed in).

4.4 Results

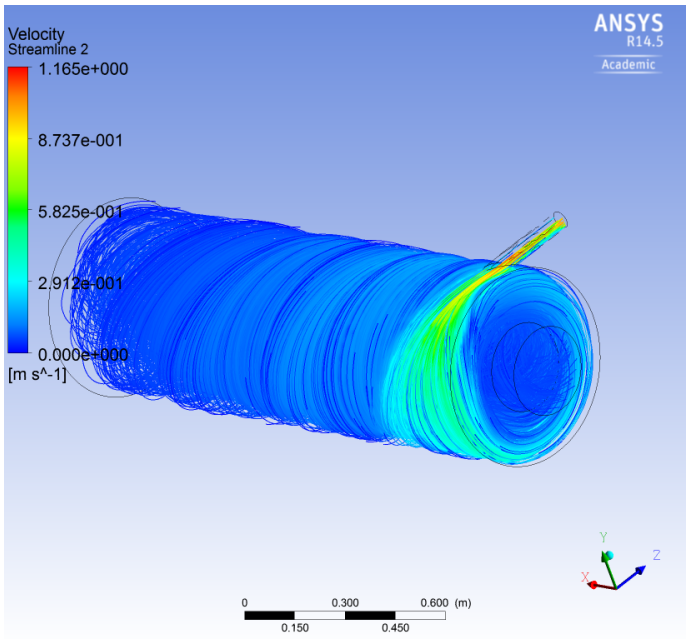

Figure 4.5. Streamlines for the 3D case

Figure 4.5 shows the 3D volume streamlines, along with the velocity contours. It can be seen that the Velocity is the highest at the inlet, but starts decreasing rapidly as soon as the fluid enters the cylindrical container. The swirling decay can also be seen as the fluid moves along the sidewall towards the dead end.

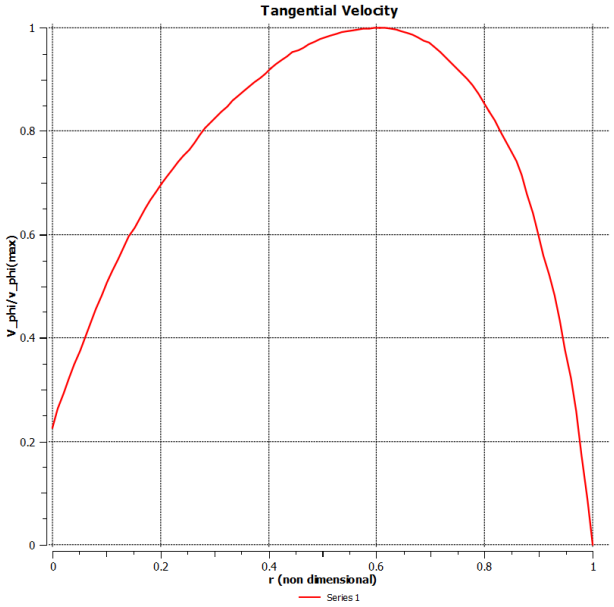

Figure 4.6. Tangential Velocity(3D).

Figure 4.6" shows the tangential velocity profile for the 3D CFD case. The behavior of the profile remains the same as the previous two cases. However, the tangential velocity at the axis of the cylinder ($r = 0$) is not zero, and has some positive value.

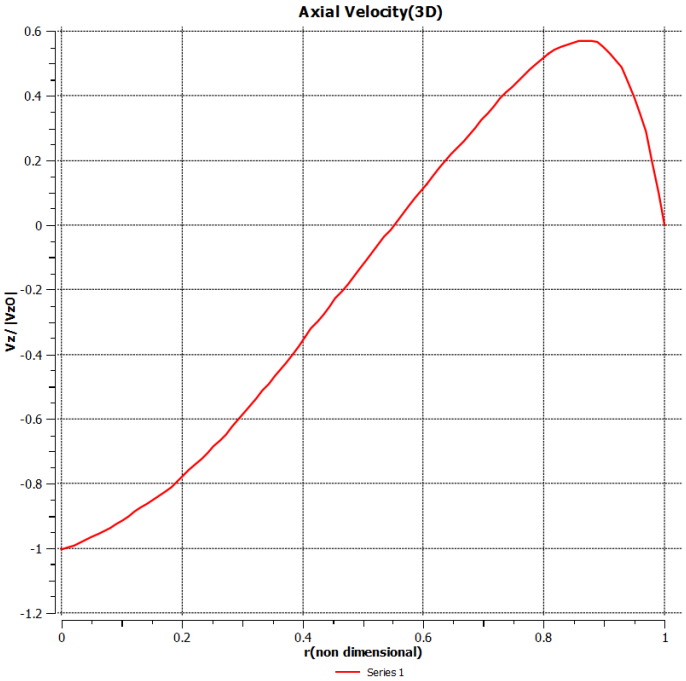

Figure 4.7. Axial Velocity(3D).

The plot for the axial velocity case behaves the same as the previous two cases. A direct comparison between the 3 cases is done in the next section.

4.5 Comparison between all the three cases

It should be noted that for the similarity analysis, turbulence was not taken into consideration. For the CFD simulations, turbulence models were used to correctly solve the solutions. This may be the source of difference between the results between them.

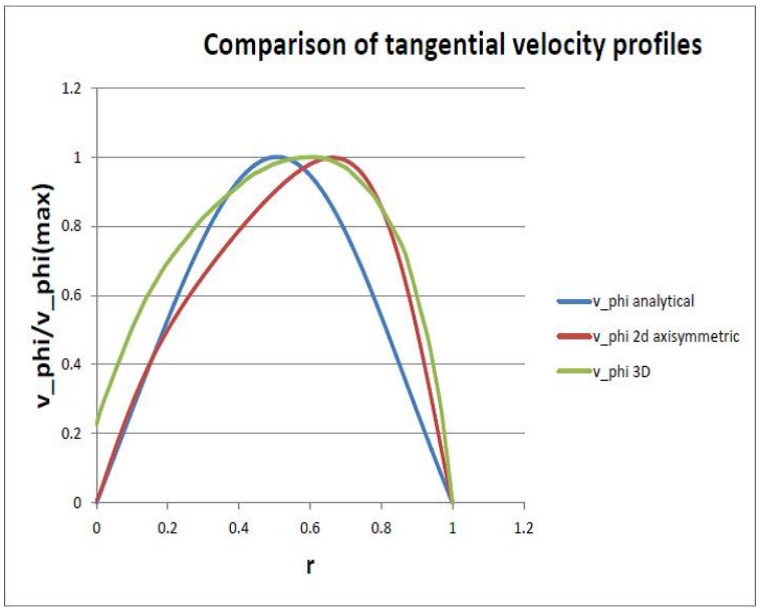

Figure 4.8. Comparison between tangential velocity profiles for all the cases.

Figure 4.8 shows the plot for the tangential velocity for all the 3 cases. The major difference between them is that the peak for the analytical solution is located right at the midpoint ($r = 0.5$) between the axis and the sidewall, while for the CFD cases, the maximum value is located slightly closer to the sidewall.

Figure 4.9 shows the plots for axial velocity for all the cases. They all behave the same, except that the CFD simulations have a higher maximum value.

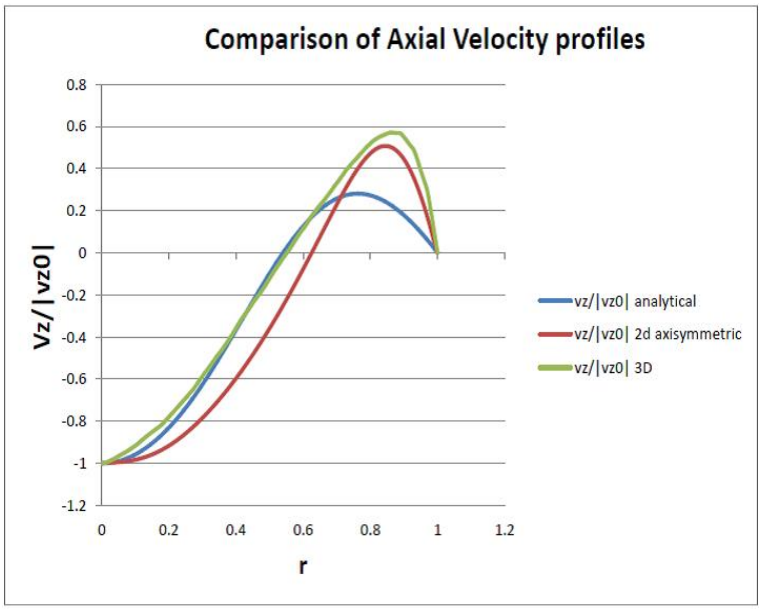

Figure 4.9. Comparison between axial velocity profiles for all the cases.

The profile for the radial velocity is not plotted in any of the cases, as the radial velocity is negligibly small in the core flow region which is being considered.

5. Conclusion

This thesis concentrates on the flow field of a swirling counterflow inside a cylindrical container where fluid is injected tangentially near the end wall that has the exhaust and is closed at the other end. A decaying swirl assumption is used to reduce the incompressible and steady Navier-Stokes equations to a set of first order ordinary differential equations, which are solved using MATLAB's boundary value problem solver 'bvp4c'. The velocity profiles are plotted in the core flow region (away from the end walls) and the pressure distribution is obtained. It is shown that that the counterflow exists because of the opposite pressure gradients at the side wall and the dead end. Computational Fluid Dynamics (CFD) simulations are then conducted of the same configuration in a steady 2D axisymmetric setup and full 3D setup using RNG (Re-Normalization Group) $k-\epsilon$ turbulence model and the results are compared. Similar velocity profiles are observed for all the three cases, with slight variations in their values.

The results obtained here are for a simple configuration with a lot of simplifications and assumptions. A more complex study can be conducted by considering the effects of compressibility, turbulence, heat addition and/or combustion, and considering a more complex geometry with different boundary conditions such as exhaust effect of having a nozzle or effects of side wall addition. The work done here provides a basic

analytical insight into the flow field of a swirling counterflow and can be used as a foundation for future work.

REFERENCES

Akiki, G. (2011). *"on the bidirectional vortex engine flowfield with arbitrary endwall injection* (Master's Thesis). Eindhoven University of Technology.

Ashley, S. (2009). *Vortex rocket engine reaps the whirlwind.* Retrieved from `http://articles.sae.org/11560/1`

Chen, J. J., & Chen, C. H. (2011). Investigation of swirling flows in mixing chambers. *Modelling and Simulation in Engineering*.

Chiaverini, M., & Kuo, K. (2007). *Fundaments of hybrid rocket combustion and propulsion* (Vol. 218). Reston, Virginia: American Institute of Aeronautics and Astronautics.

Fokeer, S. (2006). *An investigation of geometrically induced swirl applied to lean phase pneumatic flows* (Phd Thesis). The University of Nottingham.

Gupta, A. K., Lilley, D. G., & Syred, N. (1984). *Swirl flows.* Tunbridge Wells, England: Abacus Press.

Itai, Y., Ferreira, R. W. M., Guerra, D. R., & Mesquita, A. L. A. (2006). Prediction of flowfield in a curved channel. *Proceedings of the 11th Brazilian Congress of Thermal Sciences and Engineering*.

Knuth, W. H., Chiaverini, M. J., Sauer, J. A., & Gramer, D. J. (2002). Solid-fuel regression rate behavior of vortex hybrid rocket engines. *Journal of propulsion and power*.

Lopez, J. M. (2012). Three-dimensional swirling flows in a tall cylinder driven by a rotating endwall. *Physics of fluids*.

Lucca-Negro, O., & ODoherty, T. (2001). Vortex breakdown: a review. *Progress in Energy and Combustion Science*, 431-481.

Majdalani, J., & Vyas, A. (2004). Rotational axisymmetric mean flow for the vortex injection hybrid rocket engine. *40th AIAA/ASME/SAE/ASEE Joint Propulsion Conference and Exhibit*.

Mununga, L., Jacono, D. L., SÃÿrensen, N. J., Leweke, T., Thompson, C. M., & Hourigan, K. (2004). Control of confined vortex breakdown with partial rotating lids. *Journal of Fluid Mechanics*, 5-33.

Ozgen, S., & Yildiz, A. (2010). Application of box-behnken design to modeling the effect of smectite content on swelling to hydrocyclone processing of bentonites with various geologic properties. *Clays and Clay Minerals*, 431-448.

Parchen, R. R., & Steenbergen, W. (1998). An experimental and numerical study of turbulent swirling pipe flows. *Journal of Fluids Engineering*, *120*, 54-61.

Pashtrapanska, M., Jovanovic, Lienhart, H., & Durst, F. (2006). Turbulence measurements in a swirling pipe flow. *Experiments in Fluids*, *41* , 813-827.

Rocklage-Marliani, G., Schmidts, M., & Ram, V. I. V. (2003). Three-dimensional laser-doppler velocimeter measurements in swirling turbulent pipe flow. *Flow, Turbulence and Combustion*, *46*, 46-67.

Shtern, V. (2012). *Counterflows: paradoxical fluid mechanics phenomena.* New York, USA: Cambridge University Press.

Steenbergen, W. (1995). *Turbulent pipe flow with swirl* (Phd Thesis). Eindhoven University of Technology.